UC San Diego

UC San Diego Previously Published Works

Title

Signal and contrast effects due to T2 decay during k-space readout of UTE (ultrashort TE) sequences

Permalink

https://escholarship.org/uc/item/2xf3q5f1

Journal

Magnetic Resonance Imaging, 32(3)

ISSN

0730-725X

Authors

Chiang, Jing-Tzyh Alan
Carl, Michael
Du, Jiang

Publication Date

2014-04-01

DOI

10.1016/j.mri.2013.11.002

Copyright Information

This work is made available under the terms of a Creative Commons Attribution License, availalbe at https://creativecommons.org/licenses/by/4.0/

Peer reviewed

eScholarship.org Powered by the California Digital Library
University of California

NIH Public Access
Author Manuscript
Magn Reson Imaging. Author manuscript; available in PMC 2015 April 01.

Published in final edited form as:
Magn Reson Imaging. 2014 April ; 32(3): 259–269. doi:10.1016/j.mri.2013.11.002.

Signal and contrast effects due to T2 decay during k-space readout of UTE (ultrashort TE) sequences

Jing-Tzyh Alan Chiang, **Michael Carl**, and **Graeme Bydder**
Department of Radiology, University of California San Diego

Abstract

In ultrashort TE (UTE) imaging, the short T2 values of the tissues of interest are comparable to the k-space readout duration, which result in significant T2 decay during k-space readout. This decay consequently causes significant effects on signal and contrast in UTE sequences, which we evaluate in this paper using models that incorporate the gradient slew rate *slew* and maximal constant gradient strength *gmax*, in conjunction with objects of diameter *L*. The resulting signal and contrast relationships demonstrate steep signal changes between T2 values of ~50–500μs, corresponding to high T2 weighted contrast in this range. When $\gamma \cdot gmax^2/(4\pi \cdot slew) > 1/(2L)$, termed the "ramp only" regime, *gmax* has no significant effect whereas decreasing *slew* leads to decreases in signal amplitude and shifts the contrast peak to higher T2 values. When $\gamma \cdot gmax^2/(4\pi \cdot slew) < 1/(2L)$, termed the "mixed gradient" regime, both *gmax* and *slew* have significant effects, where decreases in either *gmax* or *slew* lead to lower signal amplitudes and shifts the contrast peak to higher T2 values. Under typical scan settings, the "ramp only" regime is usually dominant. Further, we demonstrate an unusual dependence of T2 weighted signal and contrast on object size, whereby objects with smaller values of *L* demonstrate lower signal amplitudes and peak contrast at higher T2 values, compared to otherwise identical objects with larger *L*. These results improve understanding of T2 weighted signal and contrast properties in short T2 tissue imaging with UTE.

INTRODUCTION

In recent years, there has been significant improvement in the ability of MR to directly image bone, the deep layers of cartilage, and other tissues with T2 values of milliseconds or less, that normally produce negligible signal due to rapid T2 decay when imaging with standard pulse sequences [1–5]. Various strategies have been developed to detect signal from such short T2 tissues. In particular, the ultrashort TE (UTE) pulse sequence is one technique where acquisition of the MR signal occurs as soon after the end of the radiofrequency (RF) excitation pulse as possible, with data sampling beginning immediately at k-space center (gradients off) and then proceeding along a radial center-out trajectory for each k-space line with data sampling occurring both during the gradient ramp as well as

© 2013 Elsevier Inc. All rights reserved.

Publisher's Disclaimer: This is a PDF file of an unedited manuscript that has been accepted for publication. As a service to our customers we are providing this early version of the manuscript. The manuscript will undergo copyediting, typesetting, and review of the resulting proof before it is published in its final citable form. Please note that during the production process errors may be discovered which could affect the content, and all legal disclaimers that apply to the journal pertain.

NIH-PA Author Manuscript
NIH-PA Author Manuscript
NIH-PA Author Manuscript

NIH-PA Author Manuscript

NIH-PA Author Manuscript

NIH-PA Author Manuscript

after the maximal gradient value is attained. This approach allows the bulk of the signal in k-space center to be sampled rapidly after RF excitation, with readout of each radial k-space line typically lasting several hundred microseconds. TE is defined as the time between the end of the RF pulse and the beginning of the read gradient, with TE as low as 8 μs being possible using special transmit-receive switching hardware, but typically ranging between 40–200μs for clinical scanners [5].

The signal and contrast properties in short T2 tissue imaging with UTE are different from conventional imaging of long T2 tissues. Due to the extremely short TE, minimal T2 decay occurs during the TE interval when imaging short T2 tissues with UTE. Instead, appreciable decay can occur during RF excitation [6] and k-space readout [7] in UTE sequences, as the duration of these intervals may be comparable to the T2 values of the tissues of interest (milliseconds or less). While the RF duration in UTE can be minimized using very short hard RF pulses (RF pulses of 100μs or less can typically give sufficient signal), the lower limits of k-space readout duration is constrained by gradient limitations to ~500μs. Therefore, depending on the RF duration, T2 decay during k-space readout can be the primary and dominant source of T2 weighted contrast in short T2 tissue imaging with UTE.

The effect on signal due to T2 decay during UTE k-space readout was previously analyzed on point sources assuming constant gradient strength [7]. However, due to gradient slew rate limitations, significant portions of k-space readout in UTE sequences actually occur during the gradient ramp prior to reaching the maximal constant gradient strength. In this manuscript, we therefore use a gradient model that includes both the ramp and maximal constant components to evaluate the differential effects on signal and contrast, of the ramp slew rate (*slew*) and the gradient constant maximal strength (*gmax*). Using radially symmetric objects of diameter *L* as source spin densities, we find that *slew* has much greater effect on signal and contrast than *gmax* when in the “ramp only” regime of $\gamma \cdot gmax^2/(4\pi \cdot slew) > 1/(2L)$, whereas both *slew* and *gmax* have effect when in the “mixed gradient” regime of $\gamma \cdot gmax^2/(4\pi \cdot slew) < 1/(2L)$. Additionally, we find that object size itself is an important parameter in determining signal and contrast, where objects of smaller *L* exhibit greater signal loss than objects of larger *L* of identical T2 values. We present below the theoretical and numerical results from our analysis, along with experimental verification using gadolinium/manganese chloride solution based short T2 phantoms.

THEORY AND SIMULATION

The effects of T2 decay occurring during k-space readout on the resulting image, is equivalent to applying a filter function on the acquired k-space data prior to Fourier transform [8]. To obtain the filter function, the time domain expression for T2 decay $e^{-t/T2}$ is reparametrized by substitution of the k-space readout trajectory **k**(t) [8]. Because UTE employs a radially symmetric “center-out” k-space trajectory that begins on a linear gradient ramp and continues after reaching the constant gradient strength [5], the k-space trajectory is quadratic in time during the gradient ramp, and linear after the constant gradient is reached:

NIH-PA Author Manuscript

NIH-PA Author Manuscript

NIH-PA Author Manuscript

$$k(t)=\begin{cases} \frac{\gamma slew}{4\pi}t^2 & for\, t \le \frac{gmax}{slew} \\ \frac{\gamma gmax^2}{4\pi slew}+\frac{\gamma}{2\pi}gmax\left(t-\frac{gmax}{slew}\right) & for\, t > \frac{gmax}{slew} \end{cases} \quad \text{Equation (1)}$$

where *t* is time, *slew* is the gradient ramp slew rate, and *gmax* is the constant gradient strength.

Substitution of this k-space trajectory into $e^{-t/T2}$ yields the following decay filter function Dec(*k*):

$$\mathrm{Dec}(k)=\begin{cases} e^{-\sqrt{\frac{4\pi k}{\gamma slew}}\frac{1}{T2}} & for\, k \le k_{ramp} \\ e^{-\left(\sqrt{\frac{4\pi k}{\gamma slew}}\frac{1}{T2}+\frac{2\pi(k-k_{ramp})}{\gamma gmax}\frac{1}{T2}\right)} & for\, k > k_{ramp} \end{cases} \quad \text{Equation (2)}$$

where $k_{ramp} = \gamma \cdot gmax^2/(4\pi \cdot slew)$ is *k* at the end of the ramp interval. Since UTE does not use refocusing pulses, Dec(*k*) is valid for both T2 and T2* decay effects. The resulting effect of Dec(*k*) on the image I(**r**) of an object with spin density s(**r**) and corresponding k-space signal S(**k**) ≡ FT[s(**r**)], is then given by:

$$\mathrm{I}(\mathbf{r})=\mathrm{FT}[\mathrm{Dec}(\mathbf{k})\mathrm{S}(\mathbf{k})] \quad \text{Equation (3)}$$

In figure 1A, we plot Dec(*k*) for varying T2 values using typical gradient values of *slew* = 70 mT/m/ms and *gmax* = 40 mT/m. When T2 is relatively long (e.g. T2 = 10ms), Dec(*k*) ≈ 1 for all *k*, and therefore has minimal effect on the final image. When T2 is short, Dec(*k*) curves demonstrate progressive decay for increasing values of *k* towards the periphery of k-space, due to the "center-out" sampling trajectory of UTE. The degree of decay becomes greater for decreasing T2 values, such that for very short T2 values, most of Dec(*k*) is essentially zero except at the most central region in k-space (see figure 1A).

To analyze and quantify the effects of Dec(*k*) on signal and contrast in UTE, we applied Dec(*k*) to a 1D "box image" model, where the source spin density s(*r*) was chosen to be a one dimensional box of length *L*, with sinc function as the associated S(*k*) (note mild Gaussian smoothing was also applied to eliminate Gibbs ringing). Dec(*k*)S(*k*) and I(*r*) of this "box image" model are shown in figures 1B–C, demonstrating increasing decay in Dec(*k*)S(*k*) and I(*r*) with decreasing T2 values. To permit detailed theoretical analysis, we also evaluated an additional "box k-space" model (similar approach to references [9,10]), where the source spin density s(*r*) is chosen to be a sinc function, with the corresponding S(*k*) to be a box function of limits $k_L = \pm 1/(2L)$ in k-space. The box function S(*k*) in k-space of this "box k-space" model is much more tractable to detailed analysis, while yielding qualitative and quantitatively similar results to the "box image" model (see below, and also references [9, 10]). In figures 1D–E, we demonstrate that decreasing T2 values also leads to increasing decay in Dec(*k*)S(*k*) and I(*r*) for the "box k-space" model.

Defining signal as the central image amplitude $M \equiv I(0)$ and contrast as $W \equiv \delta M/\delta \ln T2$ [9,11], we then calculated the dependence of *M* and *W* on T2, i.e. the T2 weighted signal and contrast relationships due to T2 decay during UTE readout. Exact solutions for *M* and *W* for

NIH-PA Author Manuscript

NIH-PA Author Manuscript

NIH-PA Author Manuscript

the “box k-space” model are given below, whereas for the “box image” model, *M* and *W* could only be obtained numerically.

$$M \equiv I(r{=}0){=}\begin{cases} \frac{LT2}{\pi}\left(\gamma slewT2 - e^{-\sqrt{\frac{2\pi}{\gamma slewL}}\frac{1}{T2}}\left(\sqrt{\frac{2\pi\gamma slew}{L}}+\gamma slewT2\right)\right) if k_{ramp} \geq k_L \\ \frac{LT2}{\pi}\left(\gamma gmax\, e^{-\frac{gmax}{slewT2}}(1 - e^{\frac{gmax}{2slewT2}-\frac{\pi}{\gamma gmaxLT2}}) - e^{-\frac{gmax}{slewT2}}(\gamma gmax{+}\gamma slewT2){+}\gamma slewT2\right) if k_{ramp} \geq k_L \end{cases} \quad \text{Equation (4)}$$

$$\begin{aligned} W \equiv \frac{\partial M}{\partial \ln T2}{=} \\ &\begin{cases} \frac{LT2^2}{\pi}\left(-\sqrt{\frac{2\pi}{\gamma slewL}}\frac{1}{T2^2}e^{-\sqrt{\frac{2\pi}{\gamma slewL}}\frac{1}{T2}}\left(\sqrt{\frac{2\pi\gamma slew}{L}}+\gamma slewT2\right) - \gamma slewe^{-\sqrt{\frac{2\pi}{\gamma slewL}}\frac{1}{T2}}+\gamma slew\right) \\ +\frac{LT2}{\pi}\left(\gamma slewT2 - e^{-\sqrt{\frac{2\pi}{\gamma slewL}}\frac{1}{T2}}\left(\sqrt{\frac{2\pi\gamma slew}{L}}+\gamma slewT2\right)\right) if k_{ramp} \geq k_L \\ \frac{LT2^2}{\pi}\left(\frac{\gamma gmax^2}{slewT2^2}e^{-\frac{gmax}{slewT2}}(1 - e^{\frac{gmax}{2slewT2}-\frac{\pi}{\gamma gmaxLT2}})\right. \\ \left. +\frac{\gamma}{2T2^2}(\frac{gmax^2}{slew} - \frac{2\pi}{\gamma L})e^{\frac{gmax}{2slewT2}-\frac{\pi}{\gamma gmaxLT2}} - \frac{\gamma gmax}{slewT2^2}e^{-\frac{gmax}{slewT2}}(gmax{+}slewT2) - \gamma slewe^{-\frac{\gamma gmax}{T2}}{+}\gamma slew\right) \\ +\frac{LT2}{\pi}\left(\gamma gmax\, e^{-\frac{gmax}{slewT2}}(1 - e^{\frac{gmax}{2slewT2}-\frac{\pi}{\gamma gmaxLT2}}) - e^{-\frac{gmax}{slewT2}}(\gamma gmax{+}\gamma slewT2){+}\gamma slewT2\right) if k_{ramp}{<}k_L \end{cases} \end{aligned} \quad \text{Equation (5)}$$

In figures 2A–B, we plot *M* and *W* versus T2 for both the “box image” and “box k-space” models, using sample gradient parameters of *slew* = 70 mT/m/ms and *gmax* = 40 mT/m, and *L* =10 mm. For *M*, significant signal losses are evident for T2 values below ~10 ms, with a particularly steep drop between ~500μs and ~50μs. For T2 values below ~10μs, *M* is negligible. Correspondingly, there is high *W* between T2 values of ~500μs and ~50μs, consistent with high T2 weighted contrast in this range. On the other hand, when T2 is greater than ~10ms or less than ~10 μs, the T2 weighted contrast *W* is essentially zero.

Similar analytic results can be obtained in 2D and 3D using disks and spheres of diameter *L* as the s(**r**) for the “box image” model, and sinc-like functions of $J_1(\pi Lr)/r$ and $(\sin(\pi Lr) - \pi Lr\cos(\pi Lr))/2\pi^2 r^3$ as the s(**r**) for the “box k-space” model. Exact equations for *M* and *W* in the 2D and 3D “box k-space” models are provided in appendix 1. *M* and *W* versus T2 curves for 2D and 3D are also plotted in figures 2A–B, showing similar curves to 1D except slight shifts to higher T2 values. Small quantitative differences between the “box object” and “box k-space” models are also present in 2D and 3D, whereas in 1D the two models yielded virtually identical results. We find empirically that good quantitative agreement between the two models in 2D and 3D can be obtained by substituting an effective diameter $L_{eff} = \alpha L$ in place of *L* in the “box k-space” model, with α=0.85 in 2D and α=0.75 in 3D.

NIH-PA Author Manuscript

NIH-PA Author Manuscript

NIH-PA Author Manuscript

Effects on signal and contrast by the gradient parameters slew and gmax: "ramp only" versus "mixed gradient" regimes

Since readout duration and k-space trajectory speeds are determined by the gradient parameters *slew* and *gmax*, these two parameters significantly influence the degree of T2 decay that occurs during UTE readout, and consequent effects on *M* and *W*. In general, higher *slew* and *gmax* values lead to faster k-space trajectories, shorter readout durations, and therefore less T2 decay effects on *M* and *W*. Conversely, lower *slew* and *gmax* values lead to slower k-space trajectories, longer readout durations, and therefore greater T2 decay and signal loss effects on *M* and *W* (see below).

Depending on the exact values of *slew* and *gmax*, two distinct behaviors exist in UTE, which we term the "ramp only" and "mixed gradient" regimes. The "ramp only" regime occurs when *slew* is sufficiently low or *gmax* is sufficiently high such that $k_{ramp} > 1/(2L)$ (i.e. $\gamma \cdot gmax^2/(4\pi \cdot slew) > 1/(2L)$); the "mixed gradient" regime occurs when *slew* is sufficiently high or *gmax* sufficiently low such that $k_{ramp} < 1/(2L)$ (i.e. $\gamma \cdot gmax^2/(4\pi \cdot slew) < 1/(2L)$). The behaviors of these two regimes can be understood conceptually using the "box k-space" model, where all of $S(k)$ is contained within the limits of $k_L = \pm 1/(2L)$. When in the "ramp only" regime, $k_{ramp} > 1/(2L)$ and therefore signal acquisition of $S(k)$ during k-space readout occurs only during the gradient ramp portion of readout, so that only *slew* affects *M* and *W* (and not *gmax*). In contrast, when $k_{ramp} < 1/(2L)$ in the "mixed gradient" regime, a significant amount of $S(k)$ signal acquisition also occurs during the maximum constant gradient portion of k-space readout, and therefore *M* and *W* demonstrate dependence on both *slew* and *gmax*. Note that the above interpretations of the "ramp only" and "mixed gradient" regimes are effective even when not using the "box k-space" model, since $1/(2L)$ is a reasonable approximation of the k-space signal extent of $S(k)$ for any given object of size *L*.

The effects of *gmax* on signal and contrast, as well as its differential effects between the "ramp only" and "mixed gradient" regimes, are illustrated in figures 3A–B where *M* and *W* are plotted for *gmax* values between 100 and 1 mT/m, with fixed *slew* = 70 mT/m/ms and *L* = 10 mm. For these fixed values of *slew* and *L*, the "ramp only" regime corresponds to *gmax* > 13 mT/m and the "mixed gradient" regime corresponds to *gmax* < 13 mT/m. In figure 3A, we see that the "ramp only" regime curves of *M* and *W* (*gmax* = 100 and 30 mT/m) are identical and overlapping, reflecting the lack of dependence on *gmax* in the "ramp only" regime. In comparison, the "mixed gradient" regime curves of *M* in figure 3A (*gmax* = 10, 3, and 1 mT/m) demonstrate increasing signal loss in *M* across all T2 values with an overall shift of the *M* curves to higher T2 values as *gmax* is decreased (note that the *gmax* = 10 mT/m curve is nearly identical to the two "ramp only" regime curves, since the value of *gmax* = 10 mT/m is still very close to the transition between the two regimes). Correspondingly, in figure 3B, we observe that the "ramp only" regime curves of *W* for *gmax* = 100 and 30 mT/m are identical and overlapping, whereas the "mixed gradient" regime curves of *W* for *gmax* = 10, 3, and 1 mT/m demonstrate shifts to higher T2 values as *gmax* is decreased. These behaviors are also illustrated by plotting the peak contrast T2 value ($T2_{maxW}$) versus *gmax* in figure 3C, where we find constant $T2_{maxW}$ in the "ramp only" regime, compared to increasing $T2_{maxW}$ for decreasing values of *gmax* in the "mixed gradient" regime.

NIH-PA Author Manuscript

NIH-PA Author Manuscript

NIH-PA Author Manuscript

In figures 4A–B, we examine the effects of *slew* on signal and contrast by plotting *M* and *W* for varying *slew* values between 1000 and 10 mT/m/ms, with fixed *gmax* = 10 mT/m and *L* = 10 mm. For these values of *gmax* and *L*, the "mixed gradient" regime occurs when *slew* > 43 mT/m/ms and the "ramp only" regime occurs when *slew* < 43 mT/m/ms. For the "mixed gradient" regime curves of *M* and *W* in figures 4A–B (*slew* = 1000, 300, and 100 mT/m/ms), we see that decreasing *slew* leads to increasing signal loss in *M* with corresponding shifts of the *M* and *W* curves to higher T2 values. For the "ramp only" regime curves of *M* and *W* in figures 4A–B (*slew* = 30 and 10 mT/m/ms), further decreases in *slew* similarly lead to increasing signal loss in *M* and corresponding shifts of the *M* and *W* curves to higher T2 values, except the changes are even more pronounced in the "ramp only" regime than the curves in the "mixed gradient" regime. Plotting $T2_{maxW}$ versus *slew* in figure 4C similarly demonstrates increasing $T2_{maxW}$ for decreasing *slew* in both the "mixed gradient" and "ramp only" regimes, with the trend more pronounced in the "ramp only" regime.

To examine whether the "ramp only" or the "mixed gradient" regime is more commonly encountered in typical scanning conditions, we evaluated a range of *slew* and *gmax* values in figure 5 to see which regime they gave rise to (with varying *L* values). We found that *slew* and *gmax* values used in typical scanning conditions (e.g. *slew* = 70–200 mT/m/ms and *gmax* = 20–40 mT/m) generally give rise to the "ramp only" regime, except when *L* is relatively small (< 3 mm). In contrast, the "mixed gradient" regime occurs only when very high values of *slew* or very low values *gmax* are in use, or when imaging very small objects of small *L*. Therefore, under typical scanning conditions, the "ramp only" regime is dominant, and the signal and contrast behaviors of *M* and *W* in UTE are largely influenced by the gradient parameter *slew* rather than *gmax*.

Dependency of signal and contrast on L

In addition to *slew* and *gmax*, another parameter that affects signal and contrast due to T2 decay during UTE readout, is the size of the object being imaged. This unusual dependency [8] occurs because larger objects have more centrally distributed S(**k**) in k-space compared to smaller objects. Since the decay filter function Dec(*k*) in UTE has greater decay in k-space periphery (see figure 1A), Dec(*k*) causes less signal loss in larger objects with more centrally distributed S(**k**) than smaller objects with more peripherally distributed S(**k**).

As a result, objects with smaller *L* demonstrate decreased signal *M* and corresponding shifts of the *M* and *W* curves to higher T2 values, when compared to objects with larger *L*. This is shown in figures 6A–B, where *M* and *W* curves are plotted for varying values of *L* = 100, 30, 10, 3, and 1mm, with fixed *slew* = 70 mT/m/ms and *gmax* = 10mT/m. In figure 6C, plotting $T2_{maxW}$ versus *L* similarly demonstrates increasing $T2_{maxW}$ for decreasing *L*. Of note, this size dependence is observed in both the "ramp only " and "mixed gradient" regimes (in figures 6A–B, the "ramp only" regime is represented by *L* = 100 and 30 mm, whereas the "mixed gradient" regime is represented by *L* = 10, 3, and 1 mm).

We note here that our analysis thus far has implicitly assumed object size *L* to be greater than the size of a single voxel Δr. This assumption *L*>Δr ensures that the limits of S(k), i.e. k_L=1/(2L), is within the data sampling boundaries of each k-space line, i.e. k_{max} = 1/(2Δr). If

NIH-PA Author Manuscript

NIH-PA Author Manuscript

NIH-PA Author Manuscript

L is smaller than the voxel size (i.e. $L<\Delta r$), then k_L is greater than k_{max}, and the portions of $S(\mathbf{k})$ extending beyond k_{max} in k-space are truncated and not sampled. This truncation effect can also significantly impact signal and contrast, leading to complex results when occurring together with T2 decay effects during readout. The combined effects of having both truncation and T2 decay during readout can be modeled by adding Trunc(**k**) to Eq. (3):

$$I(\mathbf{r})=FT[Dec(\mathbf{k})Trunc(\mathbf{k})S(\mathbf{k})] \quad \text{Equation (6)}$$

where $Trunc(\mathbf{k}) = 1$ if $k<k_{max}$ and $Trunc(\mathbf{k}) = 0$ if $k>k_{max}$. The resulting effects on signal and contrast after adding Trunc(**k**) are complex and will not be discussed in further detail here. Specific examples of such analyses have been performed for point source objects in UTE radial projection sampling trajectories [7] and Cartesian/spiral sampling trajectories [12] assuming constant gradients without ramp.

Image blurring

In addition to signal loss, T2 decay during UTE radial projection readout also causes image blurring. The amount of blurring conferred on a point source assuming a constant gradient has been calculated by Rahmer et. al. by analyzing the full-width half max of the point spread function [7]. Similarly, for our analysis, we can also calculate the blurring conferred by T2 decay during readout using the full-width half max in the "box image" model, where we define blurring as the amount of increased box size beyond its original length *L* due to blurring, i.e. ΔL = FWHM-*L*. In figure 7A, we plot ΔL for varying values of *gmax* between 100 and 1 mT/m, with fixed *slew* = 70 mT/m/ms and *L* = 10 mm. Similar to signal loss, *gmax* has no effect on blurring in the "ramp only" regime for *gmax* = 100 and 30 mT/m; whereas decreasing *gmax* in the "mixed gradient" regime for *gmax* = 10, 3 and 1 mT/m leads to increasing blurring. In figure 7B, we plot ΔL for varying values of *slew* between 1000 and 10 mT/m, with fixed *gmax* = 40 mT/m and *L* = 10 mm.

Again, similar to signal loss, there is increased blurring for decreasing *slew* of 1000, 300, and 100 mT/m/ms in the "mixed gradient" regime, as well as for decreasing *slew* of 30 and 10 mT/m/ms in the "ramp only" regime (with the effect more pronounced in the "ramp only" regime). In figure 7C, we plot ΔL for varying object sizes of *L* from 100 to 1mm, and again, we see that there is increased blurring as the object size is decreased from 100 to 1mm.

MATERIALS AND METHODS

Numerical simulations and theoretical analyses were performed using Mathematica version 8 (Wolfram Research, Champagne, Illinois). All simulations where performed assuming a FOV of 64 mm with a matrix size of 256, yielding a voxel size of 0.25mm and k_{max} = 2000 m^{-1}. Simulations with *slew* = 70 mT/m/ms and *gmax* = 40 mT/m have ramp time of 0.571 ms, constant plateau sampling time of 0.889 ms, and total sampling time of 1.46 ms for the simulation. Simulations with *slew* fixed at 70 mT/m/ms while varying *gmax* at 100, 30, 10, 3, and 1 mT/m have corresponding ramp times of 1.158, 0.428, 0.142, 0.043, 0.014 ms, constant plateau sampling times of 0, 1.351, 4.626, 15.636, 46.966 ms, and total sampling times of 1.158, 1.78, 4.769, 15.679, 46.98 ms, respectively. Simulations with *gmax* fixed at

NIH-PA Author Manuscript

NIH-PA Author Manuscript

NIH-PA Author Manuscript

10 mT/m and varying *slew* of 1000, 300, 100, 30 and 10 mT/m/ms have corresponding ramp times of 0.01, 0.033, 0.1, 0.333, 1.0 ms, constant plateau sampling times of 4.692, 4.681, 4.647, 4.531, 4.197 ms, and total sampling times of 4.702, 4.713, 4.747, 4.864, 5.197 ms, respectively. When deriving predicted signal amplitude curves for the spherical phantom experiments, we instead used FOV of 150 mm with a matrix size of 256 and k_{max} = 853.33 m^{-1} to match the experimental conditions. In addition, we also included in our simulations for the phantom experiments the small amounts of predicted amplitude loss from T2 decay during the 0.04 ms RF pulse [6] and the 0.03 ms TE interval.

We constructed short T2 phantoms by filling spherical plastic containers of inner diameters 10 mm and 38 mm, with gadolinium DTPA and manganese chloride doped water solutions. Varying concentrations of manganese chloride and gadolinium led to phantoms having a range of T2 values between 0.1 and 10 ms. We imaged these phantoms using a 3D ultrashort TE sequence on a GE 3T scanner with 40μs hard RF excitation pulse, TE 30 μs, FOV 150 mm × 150 mm, and 5000 k-space projections regridded to a 256 × 256 image matrix. One set of experiments was performed by imaging 10 mm phantoms while keeping *slew* fixed at 70 mT/m/ms while varying *gmax* at 40, 20, 10, and 5 mT/m (by setting bandwidth at 125, 62.5, 31.25, 15.63 kHz) – which led to corresponding ramp times of 0.552, 0.28, 0.144, 0.064 ms, constant plateau sampling times of 0.232, 0.888, 1.968, 4.032 ms, and total sampling times of 0.784, 1.168, 2.112, 4.096 ms, respectively. Another set of experiments was performed by imaging 10mm phantoms while keeping *gmax* fixed at 10 mT/m (bandwidth fixed at 31.25 kHz) and varying *slew* of 122, 68 and 34, and 18 mT/m/ms – which led to ramp times of 0.08, 0.144, 0.288, 0.56 ms, constant plateau sampling times of 2.0, 1.968, 1.888, 1.776 ms, and total sampling times of 2.08, 2.112, 2.176, 2.336 ms, respectively. The last set of experiments was performed by imaging both 10mm and 38mm phantoms with *slew* fixed at 70 mT/m/ms and *gmax* fixed at 10 mT/m (bandwidth 31.25 kHz) – with corresponding ramp time of 0.144 ms, constant plateau sampling time of 1.968 ms, and total sampling time of 2.112 ms.

RESULTS

We performed experimental verification of our theoretical/numerical results by scanning spherical 10mm and 38 mm diameter $MnCl_2$/gadolinium solution phantoms with a range of T2 values between ~100μs and ~10ms. A 3D UTE sequence with hard pulse excitation was utilized, with varying *slew* and *gmax* values. Sample images from our scans are given in figure 8A.

We first scanned the 10mm diameter phantoms with *slew* fixed at 70 mT/m/ms and varying *gmax* values of 40, 20, 10, and 5 mT/m. With these values of *L* and *slew*, the transition from “ramp only” to “mixed gradient” regimes occurs when *gmax* drops below 13 mT/m. The measured signal intensities are plotted in figure 8B. As expected, the *gmax* = 40 and 20 mT/m measurements do not demonstrate significant differences as they correspond to the “ramp only” regime where *gmax* has no effect. In comparison, the “mixed gradient” regime measurements with *gmax* = 10 and 5 mT/m show decreasing signal as *gmax* is decreased. The predicted theoretical curves for these values of *gmax*, *slew*, and *L* are plotted for comparison, demonstrating good agreement with the measured values.

NIH-PA Author Manuscript

NIH-PA Author Manuscript

NIH-PA Author Manuscript

We then scanned the 10mm diameter phantoms with fixed *gmax* at 10 mT/m and varying *slew* values of 122, 68 and 34, and 18 mT/m/ms. For these values of *gmax* and *L*, the transition between the "mixed gradient" to "ramp only" regimes occurs when *slew* decreases below 43 mT/m/ms. As plotted in figure 8C, decreasing *slew* leads to decreasing signal intensities in both the "mixed gradient" and "ramp only" regimes – but with the changes greater when in the "ramp only" regimes with *slew* = 30 and 15 mT/m/ms. Again, the predicted theoretical curves are in good accordance with the measured values (figure 8C).

Finally, we scanned both 10mm and 38mm diameter phantoms, with fixed *gmax* = 40 mT/m and *slew* = 70 mT/m/ms. The larger 38mm diameter phantoms demonstrate greater signal intensities compared to smaller 10mm diameter phantoms of identical T2 values (figure 8D), as predicted by our theoretical analysis. The measured values also demonstrate good accordance with predicted theoretical curves.

DISCUSSION

We modeled the T2 weighted signal and contrast properties due to decay during k-space readout for UTE sequence imaging, using a gradient model that incorporates both the gradient ramp *slew* rate and the maximal constant gradient strength *gmax*, with objects of size *L*. For the "ramp only" regime, *slew* is the primary gradient parameter affecting signal and contrast. In comparison, when in the "mixed gradient" regime typified by high *slew* values, low *gmax* values, or small object sizes *L*, both *slew* and *gmax* significantly affect signal and contrast. Typical values of *slew* and *gmax* used in scanning generally give rise to the "ramp only" regime, such that *slew* is usually the dominant parameter affecting signal and contrast behaviors due to T2 decay during UTE readout. In general, decreasing *slew* (and decreasing *gmax* when in the "mixed gradient" regime) decreases signal and shifts the contrast peak to higher T2 values. Knowing the effects of varying *slew* and *gmax* can be important in various practical scanning situations, such as: a) when comparing the slew rates of different coil sets on a scanner (one may desire a lower slew rate to reduce bioeffects such as peripheral nerve stimulation), b) when comparing the performance of different scanners using different coil sets and slew rates, and c) when varying the scanner bandwidth (which alters *gmax*) in order to adjust imaging effects on chemical shift and SNR.

Additionally, we find that the diameter *L*, an intrinsic property of the source object, also has effect on signal amplitude – where objects of decreasing *L* demonstrate decreased signal with contrast peak at higher T2 values. Although the dependence of signal and contrast on *L* is somewhat unusual, similar effects have been described in other situations where the readout duration is long compared to the T2 values of interest – e.g. imaging with EPI and FSE long echo train sequences [8,13]. Further, it has been recently demonstrated that measured phase also depends on object size in UTE imaging of short T2 tissues, due to related mechanisms [9].

The signal curves for *M* demonstrate steep slopes between T2 values from ~50us to 500us, with corresponding high contrast *W* in this range of T2 values. Since clinically relevant pathologies typically manifest as increases in T2 in the organ/tissue of interest, this suggests high inherent sensitivity of UTE imaging in disease detection for tissues with T2 values in

NIH-PA Author Manuscript

NIH-PA Author Manuscript

NIH-PA Author Manuscript

this range, such as cortical bone (T2 ~350μs). For other short T2 tissues whose T2 values fall outside of this range (e.g. tendons and ligaments of T2 ~2–3 ms), our results may also provide a method to increase contrast, by adjusting *slew* and *gmax* to modify the *W* curves and expected $T2_{maxW}$ values. We do caution, however, that adjusting *slew* and *gmax* may simultaneously lead to tradeoffs in resolution due to T2 blurring (see above section on blurring, and reference [5]), and therefore must be carefully considered.

An active area of investigation is the development of quantitative UTE-based techniques to correlate measured tissue signal intensities with disease. One such example is bone water quantification where cortical bone signal intensities measured with UTE are used to estimate proton density and cortical bone water content in osteoporosis [14, 15]. Our models should help improve proton density quantification by determining the amount of T2 weighting due to decay during readout that is embedded in the measured signal intensities. The models of T2 weighted signal and contrast determination presented in this paper should be generally beneficial in the development of current and future UTE based quantitative methods.

Recent interest in short T2 imaging has led to the use of numerous other sequences such as SWIFT, ZTE, and WASPI [1–4]. For all of these sequences, T2 decay during k-space readout should play an important and perhaps dominant role in T2 weighted signal and contrast, due to the comparable k-space readout durations and short T2 tissues. One distinction, however, is that many of these sequences begin the k-space readout with the gradient already at its maximal value *gmax* (no k-space sampling on the gradient ramp) – in which case T2 weighted signal and contrast due to decay during k-space readout can be analyzed via the same approach as described here, but with $slew=\infty$ resulting in *gmax* being the dominant gradient parameter instead. Further, since smaller objects with more peripherally distributed $S(\mathbf{k})$ will experience greater T2 decay during k-space readout via similar mechanisms, the signal and contrast dependence on object size described here should be similarly present in those other short T2 imaging techniques.

Acknowledgments

We would like to express gratitude to everyone in the Bydder MR3T laboratory for their assistance in this project. Jing-Tzyh Alan Chiang would like to acknowledge funding support from NIH grant T32-EB005970.

NIH-PA Author Manuscript

NIH-PA Author Manuscript

NIH-PA Author Manuscript

APPENDIX 1

$$M_{3D}=\begin{cases} \frac{3L^3}{\pi^3}T2\left(-\frac{1}{L^2e}-\sqrt{2\pi/T2^2 slew\ \gamma\ L}\left(\begin{array}{c}30slew^3T2^5\gamma^3\\ 30L^2slew^2T2^4\gamma^2\left(\sqrt{\frac{2\pi\ \ slew\ \gamma}{L}}+slew\ T2\ \gamma\right)\\ +30\pi\ \ L\ \ slew^2T2^3\gamma^2+10\sqrt{2L}(\pi\ \ slew\ \gamma)^{3/2}T2^2\\ +\sqrt{\frac{2\ \ slew\ \gamma}{L}}\pi^{5/2}+5\pi\ \ slew\ \ T2\ \ \gamma\end{array}\right)\right) & if\ \ k_{ramp}>1/(2L)\\ \frac{3L^3}{4\pi^3}T2\gamma\left(g\max\ \ e^{-gmax/slew\ \ T2}\left(\begin{array}{c}\frac{gmax^2\gamma^2\left(gmax^2+4gmax\ \ slew\ \ T2+8slew^2T2^2\right)}{slew^2}\\ \frac{gmax^2}{slew}-\frac{2\pi}{L\gamma}\Big/2gmax\ \ T2\\ -\frac{4e}{L^2}\left(2gmax^2L^2T2^2\gamma^2+2\pi gmax\ \ L\ \ T2\ \ \gamma+\pi^2\right)\end{array}\right)\right.\\ \left.+\frac{\gamma}{slew^2}\left(120slew^5T2^5\gamma-e^{-gmax/slew\ \ \gamma}\left(\begin{array}{c}120slew^4T2^4\gamma\left(gmax+slew\right)\\ +20gmax^2slew^2T2^2\left(gmax\ \ \gamma+3slew\ \ T2\ \ \gamma\right)\\ +gmax^4\left(gmax\ \ \gamma+5slew\ \ T2\ \ \gamma\right)\end{array}\right)\right)\right) & if\ \ k_{ramp}\le 1/(2L)\end{cases}$$

NIH-PA Author Manuscript

NIH-PA Author Manuscript

NIH-PA Author Manuscript

$$
\begin{aligned}
W_{3D} = \\
&\left\{ \frac{6L^3T2}{\pi} \left(\frac{T2}{2\pi^2} \left(-\frac{\sqrt{2\pi}}{T2^2\sqrt{slew\gamma L^5}} e^{-\sqrt{2\pi/T2^2 slew\gamma L}} \left(30L^2 slew^2 T2^4\gamma^2 \left(\sqrt{2\pi slew\gamma/L} + slew T2\gamma \right) \right. \right. \right. \right. \\
&+30\pi L slew^2 T2^3\gamma^2 \\
&+10T2^2 \sqrt{2\pi^3 slew^3\gamma^3/L} + \sqrt{2\pi^5 slew\gamma/L} + 5\pi^2 slew T2\gamma \Big) \\
&-\frac{1}{L^2} e^{-\sqrt{2\pi/T2^2 slew\gamma L}} \left(30L^2 slew^3 T2^4\gamma^3 + 120L^2 slew^2 T2^3\gamma^2 \left(\sqrt{2\pi slew\gamma/L} + slew T2\gamma \right) \right. \\
&+90\pi L slew^2 T2^2\gamma^2 + 20T2 \sqrt{2\pi^3 slew^3\gamma^3/L} + 5\pi^2 slew\gamma) + 150 slew^3 T2^4\gamma^3 \Big) \\
&+\frac{1}{2\pi^2} \left(30 slew^3 T2^5\gamma^3 - \frac{1}{L^2} e^{-\sqrt{2\pi/T2^2 slew\gamma L}} \left(30L^2 slew^2 T2^4\gamma^2 (\sqrt{2\pi slew\gamma/L} + slew T2\gamma) + 30\pi L slew^2 T2^3\gamma^2 \right. \right. \\
&\left. \left. \left. \left. +10T2^2 \sqrt{2\pi^3 slew^3\gamma^3/L} + \sqrt{2\pi^5 slew\gamma/L} + 5\pi^2 slew T2\gamma \right) \right) \right) if\, k_{ramp} > 1/(2L) \\
&\frac{6L^3T2}{\pi} \left(\frac{\gamma}{8\pi^2} \left(e^{-gmax/(slew T2)} gmax \left(\frac{gmax^2\gamma^2(gmax^2 + 4slew T2 gmax + 8slew^2 T2^2)}{slew^2} \right. \right. \right. \\
&\left. \left. - \frac{4e^{\left(\frac{gmax^2}{slew} - \frac{2\pi}{L\gamma}\right)/2gmax T2} (2gmax^2 L^2 T2^2\gamma^2 + 2\pi gmax LT2\gamma + \pi^2)}{L^2} \right) \right. \\
&+\frac{\gamma}{slew^2} \left(120 slew^5 T2^5\gamma - e^{-gmax/T2slew} (5slew T2\gamma + gmax\gamma) gmax^4 \right. \\
&+20 slew^2 T2^2 (3slew T2\gamma + gmax\gamma) gmax^2 \\
&\left. \left. +120 slew^4 T2^4 (slew T2\gamma + gmax\gamma) \right) \right) \\
&+\frac{\gamma T2}{8\pi^2} \left(\frac{e^{-gmax/(slew T2)} gmax^2}{slew T2^2} \left(\frac{gmax^2\gamma^2(gmax^2 + 4slew T2 gmax + 8slew^2 T2^2)}{slew^2} \right. \right. \\
&\left. \left. - \frac{4e^{\left(\frac{gmax^2}{slew} - \frac{2\pi}{L\gamma}\right)/2gmax T2} (2gmax^2 L^2 T2^2\gamma^2 + 2\pi gmax LT2\gamma + \pi^2)}{L^2} \right) \right. \\
&+e^{-gmax/(slew T2)} gmax \left(\frac{gmax^2\gamma^2(16T2 slew^2 + 4gmax\ slew)}{slew^2} \right. \\
&-\frac{4e^{\left(\frac{gmax^2}{slew} - \frac{2\pi}{L\gamma}\right)/2gmax T2} (4gmax^2 L^2 T2\gamma^2 + 2\pi gmax L\gamma)}{L^2} \\
&\left. \left. +\frac{2e^{\left(\frac{gmax^2}{slew} - \frac{2\pi}{L\gamma}\right)/2gmax T2} \left(\frac{gmax^2}{slew} - \frac{2\pi}{L\gamma}\right) (2gmax^2 L^2 T2^2\gamma^2 + 2\pi gmax LT2\gamma + \pi^2)}{gmax L^2 T2^2} \right) \right. \\
&+\frac{\gamma}{slew^2} \left(600 T2^4\gamma slew^5 - e^{-gmax/(slew T2)} \sqrt{\frac{gmax^2\gamma}{slew}} \left((5slew T2\gamma + gmax\gamma) gmax^4 \right. \right. \\
&+20 slew^2 T2^2 (3slew T2\gamma + gmax\gamma) gmax^2 \\
&\left. \left. \left. \left. +120 slew^4 T2^4 (slew T2\gamma + gmax\gamma) \right) \right) \right) \right) if\, k_{ramp} \leq 1/(2L)
\end{aligned}
$$

NIH-PA Author Manuscript

NIH-PA Author Manuscript

NIH-PA Author Manuscript

$$M_{2D}=\begin{cases}\frac{2L^2}{\pi^2}T2\left(3slew^2T2^3\gamma^2-e^{-\sqrt{2\pi/T2^2\ \ slew\ \ \gamma\ \ L}}\left(\begin{array}{c}3slew\ \ T2\ \ \gamma\,(L,\ \ ,slew,\ \ ,T,2,\ \ ,\gamma,+,\sqrt{2\pi L\ \ slew\ \ \gamma})\\+\sqrt{\frac{2\pi^3\,slew\ \ \gamma}{L}}+3\pi\ \ slew\ \ T2\ \ \gamma\end{array}\right)\right)\\ \quad if\ \ k_{ramp}>1/\,(2L)\\ \frac{L^2\gamma}{\pi^2}T2\left(\begin{array}{c}\frac{e^{-gmax/(slew\ \ T2)}\left(-gmax^2(gmax\ \ \gamma+3slew\ \ T2\ \ \gamma)-6slew^2T2^2(gmax\ \ \gamma+slew\ \ T2\ \ \gamma)\right)}{slew}\\+\frac{gmax^2\gamma\ \ e^{-gmax/(slew\ \ T2)}(gmax+2slew\ \ T2)}{slew}-\frac{2gmax(gmax\ \ L\ \ T2\ \ \gamma+\pi)e^{-\frac{\pi}{gmax\ \ L\ \ T2\ \ \gamma}-\frac{gmax}{2slew\ \ T2}}}{L}+6slew^2T2^3\gamma\end{array}\right)\\ \quad if\ \ k_{ramp}\le 1/\,(2L)\end{cases}$$

$$W_{2D}=\begin{cases}\frac{4L^2T2}{\pi}\left(\begin{array}{c}\frac{T2}{2\pi}\left(\begin{array}{c}-\frac{e^{-\sqrt{2\pi/T2^2\ \ slew\ \ \gamma\ \ L}}\left(3L\ \ slew^2T2^2\gamma^2+6\ \ slew\ \ T2\ \ \gamma\left(L\ \ slew\ \ T2\ \ \gamma+\sqrt{2\pi L\ \ slew\ \ \gamma}\right)+3\pi\ \ slew\ \ \gamma\right)}{L}\\-\frac{\sqrt{\frac{2\pi}{L^3}}e^{-\sqrt{2\pi/T2^2slew\ \ \gamma\ \ L}}\left(3slew\ \ T2\ \ \gamma\left(L\ \ slew\ \ T2\ \ \gamma+\sqrt{2\pi L\ \ slew\ \ \gamma}\right)+\sqrt{\frac{2\pi^3slew\ \ \gamma}{L}}+3\pi slew\ \ T2\ \ \gamma\right)}{T2^2\sqrt{slew\ \ \gamma}}\\+9\ \ slew^2T2^2\gamma^2\end{array}\right)\\+\frac{3\ \ slew^2T2^3\gamma^2}{2\pi}\\-\frac{e^{-\sqrt{2\pi/T2^2\ \ slew\ \ \gamma\ \ L}}\left(3slew\ \ T2^2\gamma\left(L\ \ slew\ \ T2\ \ \gamma+\sqrt{2\pi L\ \ slew\ \ \gamma}\right)+\sqrt{\frac{2\pi^3slew\ \ \gamma}{L}}+3\pi slew\ \ T2\ \ \gamma\right)}{2\pi L}\end{array}\right)\\ \quad if\ \ k_{ramp}>1/\,(2L)\\ \frac{4L^2T2}{\pi}\left(\begin{array}{c}\frac{\gamma}{4\pi}\left(\begin{array}{c}\frac{e^{-gmax/(slew)}\left(-gmax^2(gmax\ \ \gamma+3slew\ \ T2\ \ \gamma)-6slew^2T2^2(gmax\ \ \gamma+slew\ \ T2\ \ \gamma)\right)}{slew}\\+\frac{gmax^2\gamma\ \ e^{-gmax/(slew\ \ T2)}(gmax+2slew\ \ T2)}{slew}-\frac{2gmax(gmax\ \ L\ \ T2\ \ \gamma+\pi)e^{-\frac{\pi}{gmax\ \ L\ \ T2\ \ \gamma}-\frac{gmax}{2slew\ \ T2}}}{L}+6slew^2T2^3\gamma\end{array}\right)\\+\frac{T2\ \ \gamma}{4\pi}\left(\begin{array}{c}\frac{gmax^3\gamma\ \ e^{-gmax/(slew\ \ T2)}(gmax+2slew\ \ T2)}{slew^2\ \ T2^2}-2gmax^2\gamma\ \ e^{-\frac{\pi}{gmax\ \ L\ \ T2\ \ \gamma}-\frac{gmax}{2slew\ \ T2}}\\+\sqrt{\frac{gmax^2\gamma}{slew}}\frac{e^{-gmax/(slew\ \ T2)}\left(-gmax^2(gmax\ \ \gamma+3slew\ \ T2\ \ \gamma)-6slew^2T2^2(gmax\ \ \gamma+slew\ \ T2\ \ \gamma)\right)}{slew\ \ T2^2\sqrt{slew\ \ \gamma}}\\+\frac{e^{-gmax/(slew\ \ T2)}\left(-12\ \ slew^2T2(gmax\ \ \gamma+slew\ \ T2\ \ \gamma)-3gmax^2slew\ \ \gamma-6slew^3\ \ T2^2\gamma\right)}{slew}\\+2gmax^2\gamma e^{-gmax/(slew\ \ T2)}\\-\frac{2gmax(gmax\ \ L\ \ T2\ \ \gamma+\pi)e^{-\frac{\pi}{gmax\ \ L\ \ T2\ \ \gamma}-\frac{gmax}{2slew\ \ T2}}\left(\frac{\pi}{gmax\ \ L\ \ T2^2\gamma}+\frac{gmax}{2slew\ \ T2^2}\right)}{L}\\+18slew^2T2^2\gamma\end{array}\right)\end{array}\right)\\ \quad if\ \ k_{ramp}\le 1/\,(2L)\end{cases}$$

References

1. Grodzki DM, Jakob PM, Heismann B. Ultrashort echo time imaging using pointwise encoding time reduction with radial acquisition (PETRA). Magn Reson Med. 2012 Feb; 67(2):510–518. [PubMed: 21721039]
2. Idiyatullin D, Corum C, Park JY, Garwood M. Fast and quiet MRI using a swept radiofrequency. J Magn Reson. 2006 Aug; 181(2):342–349. [PubMed: 16782371]
3. Weiger M, Pruessmann KP, Hennel F. MRI with zero echo time: hard versus sweep pulse excitation. Magn Reson Med. 2011 Aug; 66(2):379–389. [PubMed: 21381099]
4. Wu Y, Hrovat MI, Ackerman JL, Reese TG, Cao H, Ecklund K, Glimcher MJ. Bone matrix imaged in vivo by water- and fat-suppressed proton projection MRI (WASPI) of animal and human subjects. J Magn Reson Imaging. 2010 Apr; 31(4):954–963. [PubMed: 20373441]
5. Tyler DJ, Robson MD, Henkelman RM, Young IR, Bydder GM. Magnetic resonance imaging with ultrashort TE (UTE) PULSE sequences: technical considerations. J Magn Reson Imaging. 2007 Feb; 25(2):279–289. [PubMed: 17260388]

NIH-PA Author Manuscript

NIH-PA Author Manuscript

NIH-PA Author Manuscript

6. Carl M, Bydder M, Du J, Takahashi A, Han E. Optimization of RF excitation to maximize signal and T2 contrast of tissues with rapid transverse relaxation. Magn Reson Med. 2010 Aug; 64(2):481–490. [PubMed: 20665792]
7. Rahmer J, Börnert P, Groen J, Bos C. Three-dimensional radial ultrashortecho-time imaging with T2 adapted sampling. Magn Reson Med. 2006 May; 55(5):1075–1082. [PubMed: 16538604]
8. Haacke, EM.; Brown, RW.; Thompson, MR.; Venkatesan, R. Magnetic Resonance Imaging: Physical Principles and Sequence Design. New York: Wiley-Liss; 1999.
9. Carl M, Chiang JT. Investigations of the origin of phase differences seen with ultrashort TE imaging of short T2 meniscal tissue. Magn Reson Med. 2012 Apr; 67(4):991–1003. [PubMed: 21898582]
10. Nishimura, D. Principles of Magnetic Resonance Imaging. Stanford, CA: Stanford University; 2010.
11. Yokoo T, Bae WC, Hamilton G, Karimi A, Borgstede JP, Bowen BC, Sirlin CB, Chung CB, Crues JV, Bradley WG, Bydder GM. A quantitative approach to sequence and image weighting. J Comput Assist Tomogr. 2010 May-Jun;34(3):317–331. [PubMed: 20498530]
12. Qin Q. Point spread functions of the T2 decay in k-space trajectories with long echo train. Magn Reson Imaging. 2012 Oct; 30(8):1134–1142. [PubMed: 22817958]
13. Constable RT, Gore JC. The loss of small objects in variable TE imaging: implications for FSE, RARE, and EPI. Magn Reson Med. 1992 Nov; 28(1):9–24. [PubMed: 1435225]
14. Du J, Carl M, Bydder M, Takahashi A, Chung CB, Bydder GM. Qualitative and quantitative ultrashort echo time (UTE) imaging of cortical bone. J Magn Reson. 2010 Dec; 207(2):304–311. [PubMed: 20980179]
15. Techawiboonwong A, Song HK, Leonard MB, Wehrli FW. Cortical bone water: in vivo quantification with ultrashort echo-time MR imaging. Radiology. 2008 Sep; 248(3):824–833. [PubMed: 18632530]

NIH-PA Author Manuscript
NIH-PA Author Manuscript
NIH-PA Author Manuscript

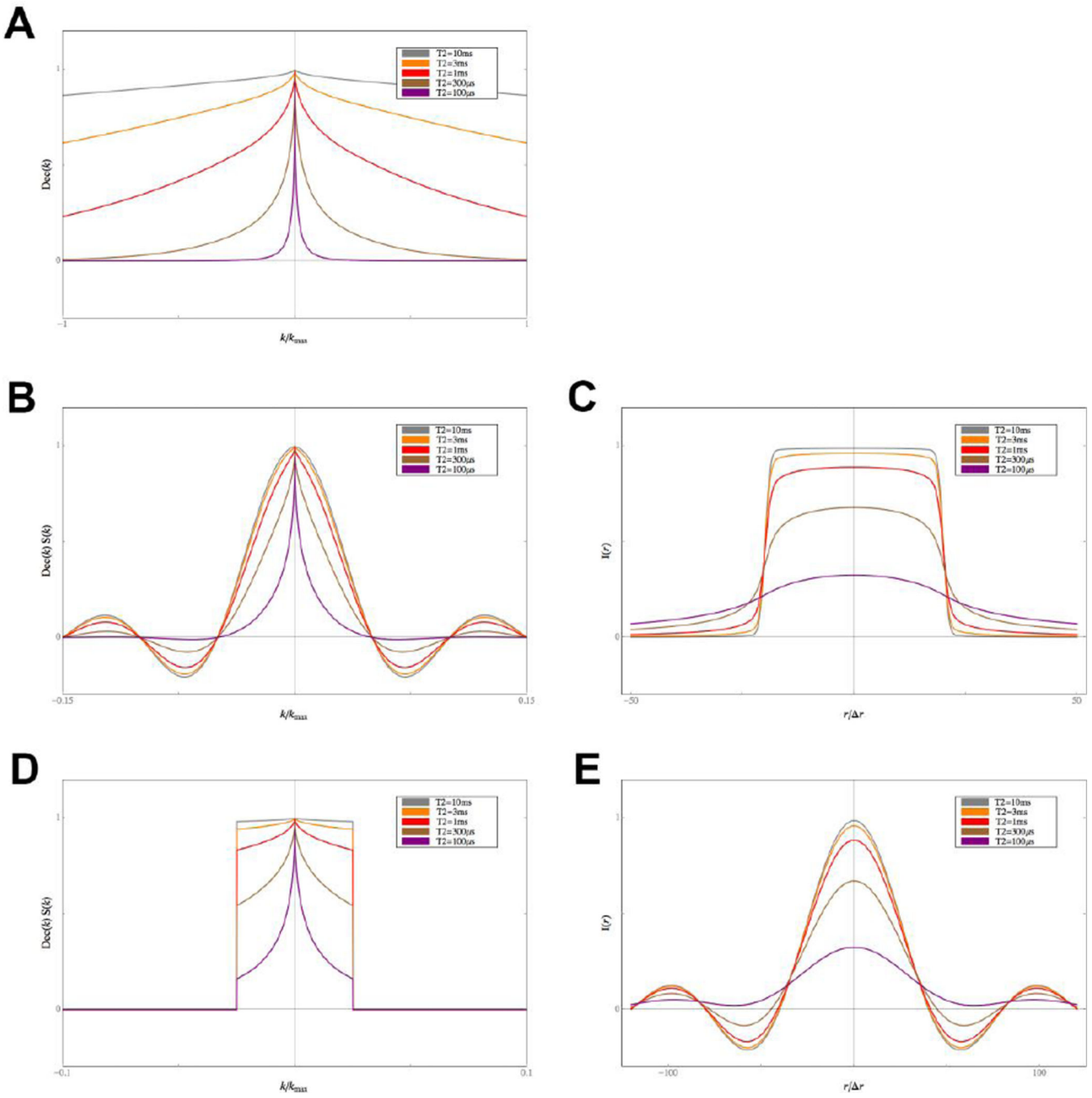

Fig 1. Effects of the filter function Dec(*k*) on k-space signal S(*k*) and the resulting image I(*r*)

A) Dec(*k*), the k-space filter function given in equation 2, represents the effects of T2 decay during UTE k-space readout. **B–C)** Dec(*k*)S(*k*) and I(*r*) = FT[Dec(*k*)S(*k*)] in the "box image" model showing increasing decay for decreasing T2 values. **D–E)** Dec(*k*)S(*k*) and I(*r*) = FT[Dec(*k*)S(*k*)] in the "box k-space" model showing increasing decay for decreasing T2 values. Length is displayed in units of voxel size Δr, and k-space is displayed in units of k_{max} = 1/(2Δr). Parameters for Figure 1 were set at: *slew* = 70 mT/m/ms, *gmax* = 40mT/m, *L* = 10mm, Δr = 0.25mm, and k_{max} = 2000 m^{-1}.

NIH-PA Author Manuscript

NIH-PA Author Manuscript

NIH-PA Author Manuscript

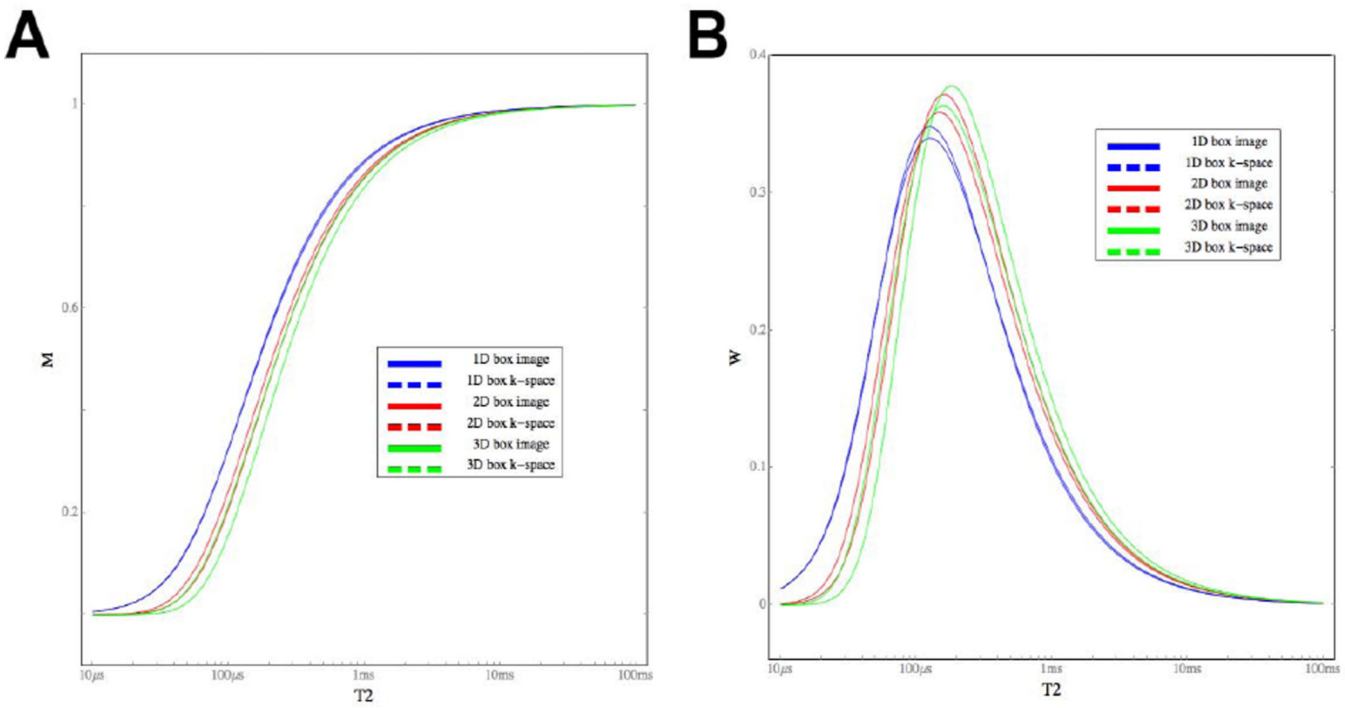

Figure 2. T2 weighted signal and contrast curves due to the effects of Dec(*k*)

A) Signal *M* versus T2 (with *L* =10 mm, *slew* = 70 mT/m/ms, *gmax* = 40 mT/m), for 1D/2D/3D "box image" and "box k-space" models. Steep signal drop occurs between T2 ~500μs and 50μs. **B)** Contrast *W* versus T2 (with *L* =10 mm, *slew* = 70 mT/m/ms, *gmax* = 40 mT/m). Corresponding to the steep portions of the *M* versus T2 curves, there is high *W* for T2 values between ~500μs and 50μs.

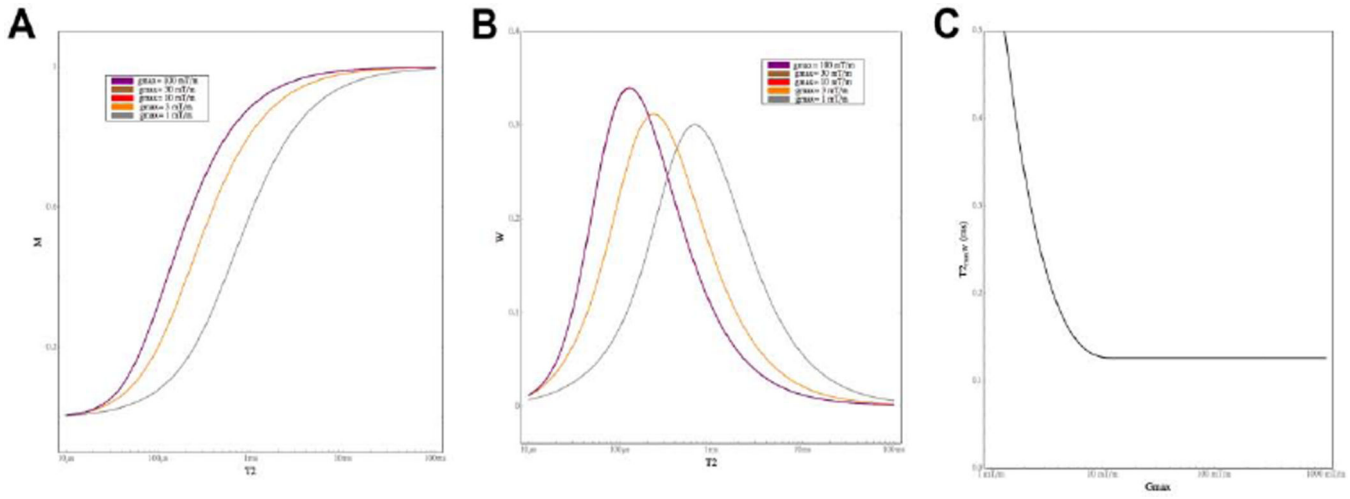

Fig 3. The effects of *gmax* on signal and contrast

A) *M* versus T2 curves for *gmax* = 100, 30, 10, 3, and 1 mT/m (with *slew* = 70 mT/m/ms, *L* =10 mm). The transition from "ramp only" to "mixed gradient" regimes occurs at *gmax* =13 mT/m, such that the *gmax* = 100 and 30 mT/m curves correspond to the "ramp only" regime and the *gmax* = 10, 3, and 1 mT/m curves correspond to the "mixed gradient" regime. The "ramp only" regime curves are identical and overlapping because *gmax* has no effect in the "ramp only" regime. In the "mixed gradient" regime, lower *gmax* causes decreased signal *M* at all T2 values. Note that the *gmax* = 10 mT/m curve is very close to the transition between the two regimes, such that it is adjacent to but not identical to the two "ramp only" regime curves. **B)** Corresponding *W* versus T2 curves. The "ramp only" regime curves for *gmax* = 100 and 30 mT/m are identical and overlapping. In the "mixed gradient" regime, the curves are shifted to higher T2 values as *gmax* is decreased. **C)** $T2_{maxW}$, the T2 value at which peak contrast *W* occurs, is plotted versus *gmax*. $T2_{maxW}$ is constant when in the "ramp only", whereas $T2_{maxW}$ increases for decreasing *gmax* in the "mixed gradient" regime.

NIH-PA Author Manuscript
NIH-PA Author Manuscript
NIH-PA Author Manuscript

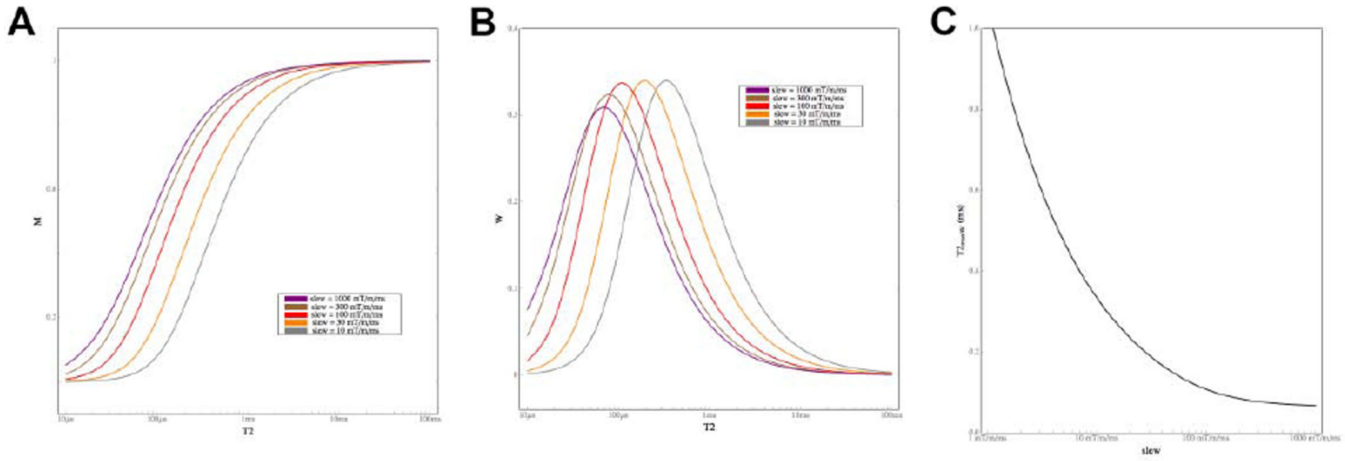

Fig 4. The effects of *slew* on signal and contrast

A) *M* versus T2 curves for *slew* = 1000, 300, 100, 30, and 10 mT/m/ms (with *gmax* = 10 mT/m/ms, *L* =10 mm). The transition from "mixed gradient" to "ramp only" regimes occurs at *slew* =43 mT/m/ms, such that the *slew* = 1000, 300, and 100 mT/m/ms curves correspond to the "mixed gradient" regime and the *slew* = 30 and 10 mT/m/ms curves correspond to the "ramp only" regime. In both regimes, lower *slew* causes decreased signal *M* at all T2 values. **B)** Corresponding *W* versus T2 curves. In both regimes, the curves are shifted to higher T2 values as *slew* is decreased. **C)** $T2_{maxW}$ versus *slew*. $T2_{maxW}$ increases for decreasing *slew* in both regimes.

NIH-PA Author Manuscript NIH-PA Author Manuscript NIH-PA Author Manuscript

NIH-PA Author Manuscript

NIH-PA Author Manuscript

NIH-PA Author Manuscript

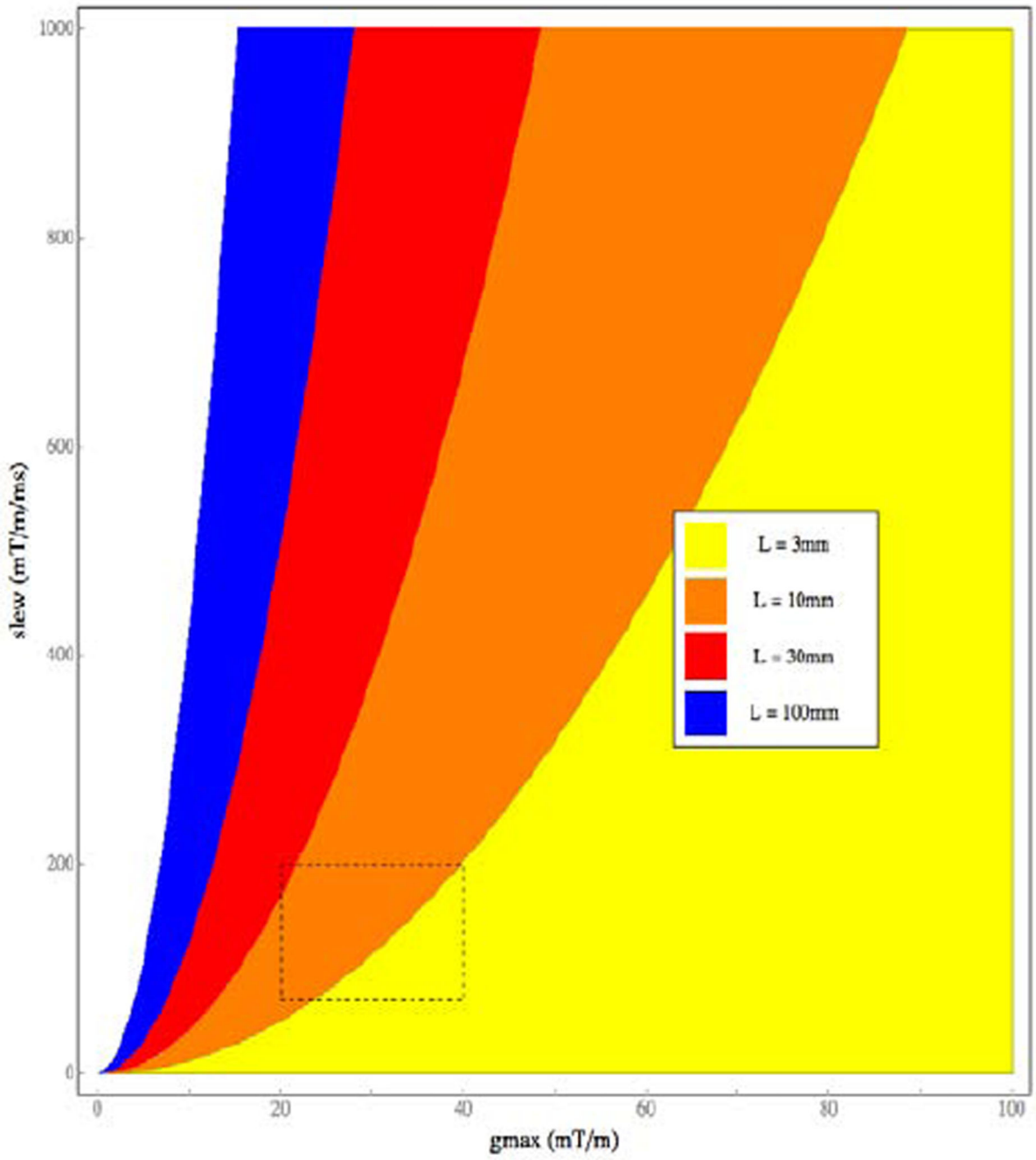

Fig 5. Combinations of *gmax* and *slew* that correspond to "ramp only" versus "mixed gradient" regimes

The range of *gmax* and *slew* values that correspond to the "ramp only" regime are color-shaded, for *L* = 100, 30, 10, and 3 mm. A dashed box surrounds a region of *slew* between 70–200 mT/m/ms and *gmax* between 20–40 mT/m, signifying sample "typical" scanning conditions.

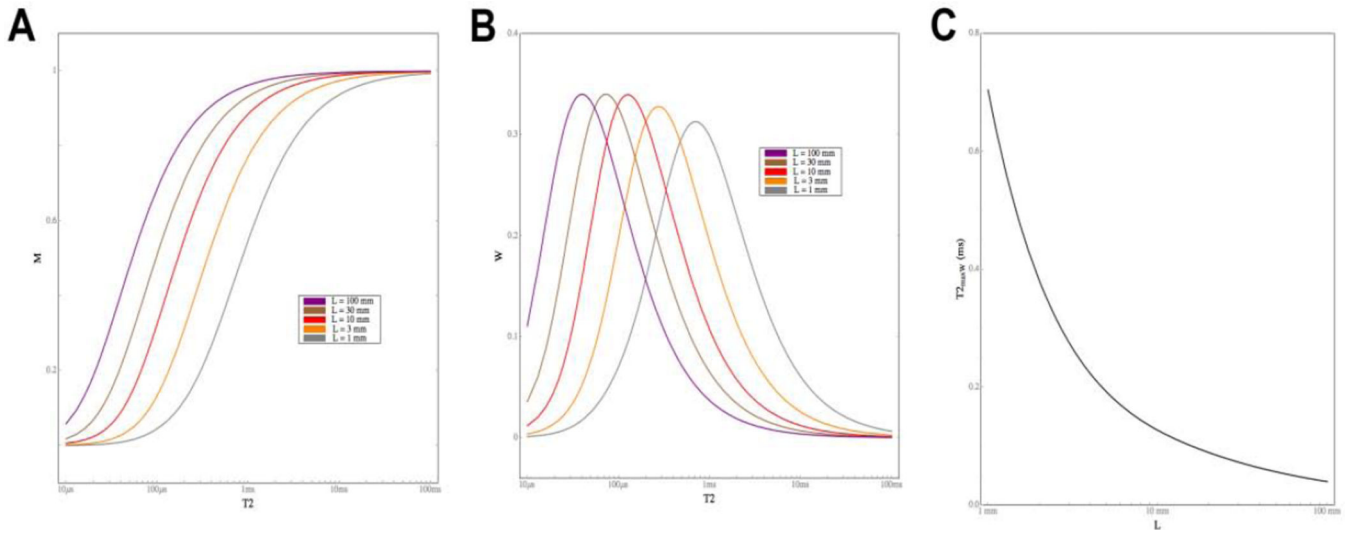

Figure 6. The effects of object size *L* on signal and contrast

A) *M* versus T2 curves for *L* = 100, 30, 10, 3, and 1 mm (with *gmax* = 10 mT/m, *slew* = 70 mT/m/ms). The "ramp only" regime is represented by the *L* = 100 and 30 mm curves, whereas the "mixed gradient" regime is represented by *L* = 10, 3, and 1 mm curves. In both regimes, smaller *L* causes decreased signal *M* at all T2 values. **B)** Corresponding *W* versus T2 curves. In both regimes, the curves are shifted to higher T2 values as *L* is decreased. **C)** $T2_{maxW}$ versus *L* curves. $T2_{maxW}$ increases for decreasing *L* in both regimes.

NIH-PA Author Manuscript
NIH-PA Author Manuscript
NIH-PA Author Manuscript

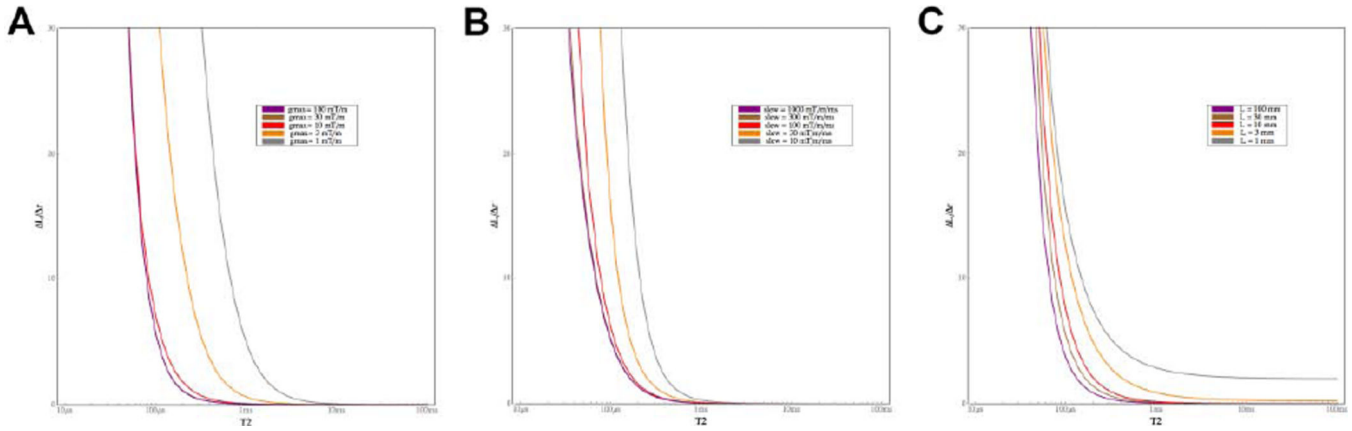

Figure 7. Blurring effects due to T2 decay during UTE readout

Blurring is defined as the amount of increased box size (at full-width half max) beyond its original length *L*, i.e. Δ*L* = FWHM-*L* (see text for full details). Similar to signal loss, there is more blurring as when *gmax* is decreased in the "mixed gradient" regime, when *slew* is decreased, and for smaller *L*. **A)** Δ*L* versus T2 curves for *gmax* = 100, 30, 10, 3, and 1 mT/m (with *slew* = 70 mT/m/ms, *L* =10 mm). **B)** Δ*L* versus T2 curves for *slew* = 1000, 300, 100, 30, and 10 mT/m/ms (with *gmax* = 40 mT/m, *L* =10 mm). **C)** Δ*L* versus T2 curves for *L* = 100, 30, 10, 3, and 1 mm (with *gmax* = 40 mT/m, *slew* = 70 mT/m/ms).

NIH-PA Author Manuscript
NIH-PA Author Manuscript
NIH-PA Author Manuscript

NIH-PA Author Manuscript
NIH-PA Author Manuscript
NIH-PA Author Manuscript

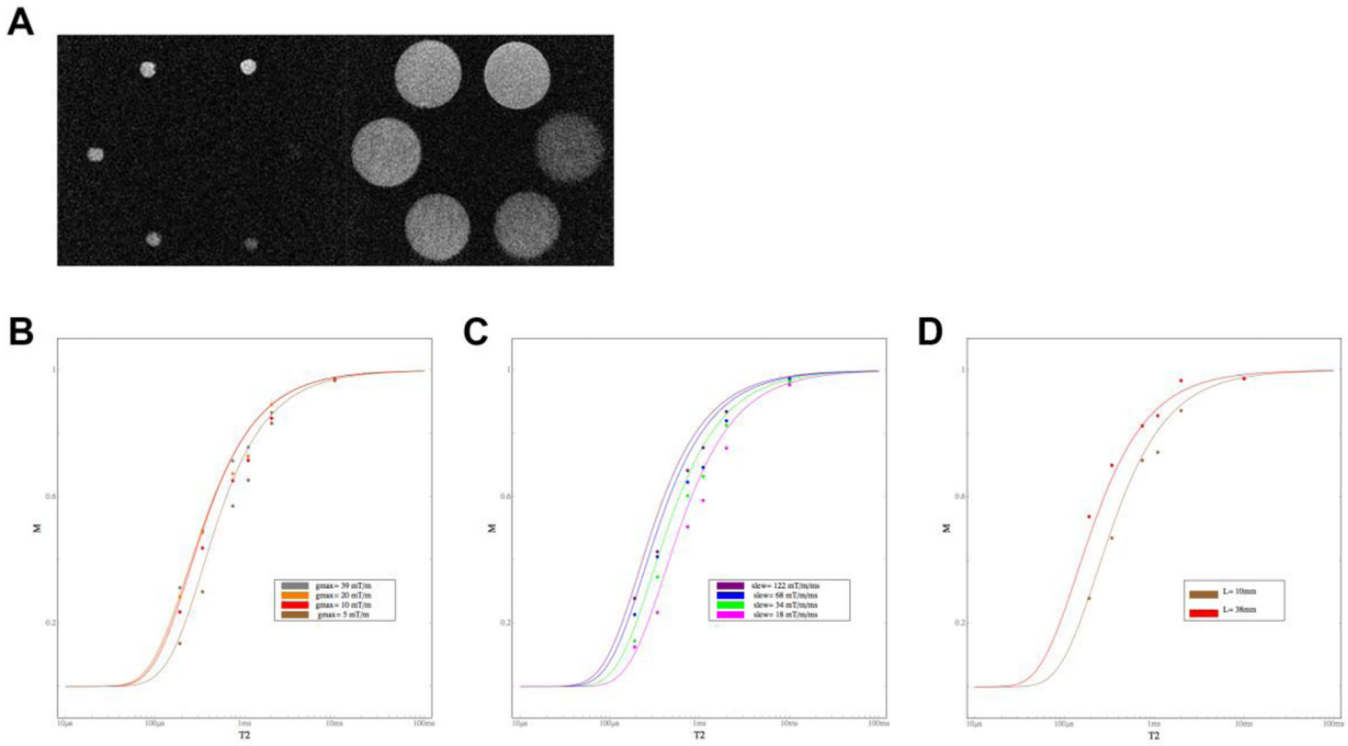

Figure 8. Experimental validation using spherical short T2 solution phantoms

A) Sample 3D UTE images of 10mm and 38mm diameter spherical phantoms of varying gadolinium/manganese chloride concentrations, with T2 values of 10.1, 2.0, 1.1, 0.74, 0.34, and 0.19ms. **B)** Measured signal intensities from 10mm diameter phantoms are plotted ("•") at varying values of *gmax* = 40, 20, 10, and 5 mT/m (with *slew* = 70 mT/m/ms). Good agreement with predicted theoretical curves is demonstrated, including in the "ramp only" regime measurements for *gmax* = 40 and 20 mT/m (the transition from "ramp only" to "mixed gradient" regime occurs at *gmax* = 13 mT/m). **C)** Measured signal intensities from 10mm diameter phantoms ("•") for varying *slew* = 122, 68, 34, and 18 mT/m/ms, show good agreement with predicted theoretical curves. **D)** Measured signal intensities from 10mm and 38mm diameter phantoms ("•") with *slew* of 70 mT/m/ms and *gmax* of 40 mT/m. The smaller 10mm diameter phantoms demonstrate lower signal intensities compared to the larger 38mm diameter phantoms, in good agreement with theoretically predicted curves.